# Cohesive zone model identification on mode I bonded assembly: sensitivity analysis

Agathe Jaillon, Julien Jumel, Eric Paroissien, Frederic Lachaud

# COHESIVE ZONE MODEL IDENTIFICATION ON MODE I BONDED ASSEMBLY: SENSITIVITY ANALYSIS

Agathe Jaillon[1], Julien Jumel[2], Éric Paroissien[3], Frédéric Lachaud[4].

[1] Institut Clément Ader, Université de Toulouse, CNRS-INSA-ISAE-Mines Albi-UPS, UMR 5312, Toulouse, France, agathe.jaillon@isae.fr, http://institut-clement-ader.org

[2] I2M, Université de. Bordeaux, Arts et Métiers Paris Tech, CNRS, UMR 5295, Talence, France, julien.jumel@u-bordeaux.fr, https://www.i2m.u-bordeaux.fr/en

[3] Institut Clément Ader, Université de Toulouse, CNRS-INSA-ISAE-Mines Albi-UPS, UMR 5312, Toulouse, France, eric.paroissien@isae.fr, http://institut-clement-ader.org

[4] Institut Clément Ader, Université de Toulouse, CNRS-INSA-ISAE-Mines Albi-UPS, UMR 5312, Toulouse, France, frederic.lachaud@isae.fr, http://institut-clement-ader.org

**Keywords:** DCB, Cohesive zone model, Chi-square minimization, Sensitivity, Confidence interval

**ABSTRACT**

Adhesive bonding is usually modelled using cohesive zone models (CZM) which are defined by traction-separation (TS) law. For mode I loading condition these phenomenological laws simply represent the evolution of the peel stress as a function of the two adherends relative displacement normal to the joint. However, TS law shape is often empirically chosen rather than being measured. The uncertainty on parameter estimation is generally not indicated even though it strongly influences the reliability of the bonded joint strength prediction. Moreover there are several mechanical data that can be obtained experimentally from crack initiation and propagation experiments on a Double Cantilever Beam Test (DCB). In general, TS parameters are chosen from load-displacement curves, which is the most straightforward mechanical response to obtain. However, the development of digital image correlation has enabled to access more numerous data, such as adherends' deflection and rotation along the overlap and at loading point. The latter can be directly used to obtain the J integral. Adherends' deformation can also be measured through the use of resistive strain gauges. Therefore, these different identification methods need to be compared in terms of parameter estimation confidence intervals. To do so, a numerical test campaign has been carried out for each mechanical response (i.e. load-displacement, J integral, and strain measurement) a synthetic noise is added to the nominal response in order to artificially represent measurement data. The noisy response is then used for the identification of the parameters using a nonlinear least square minimization. Once the data are fitted, the parameters sensitivity and confidence intervals can then be established enabling the rigorous evaluation of these different techniques to capture the best parameters for a chosen CZM shape.

## 1 INTRODUCTION

Adhesive bonding has been subjected to a growing interest in the transport sector. But, as its main problematic is mass reduction, materials repartition and junction strategies need to be redesigned. Thereby, adhesive bonding can appear as a good alternative. Indeed, it enables the assembly of different materials, such as composites and metals, and offers a very competitive strength-to-mass ratio. However, structural adhesive bonding suffers from a general lack of confidence from the aeronautical sector. Thus, the development of robust models could enable its establishment as a viable solution for structural bonding.

Currently, adhesive bonding is in general modelled using Cohesive Zone Models (CZM) which have been used for the evaluation of the failure conditions of interfaces in laminates and later on bonded joints. These models have been studied extensively from a theoretical and numerical point of view and many contributions have used them for failure load prediction of many different materials [1]. They represent the cohesive stresses versus interface relative displacement evolution and could be

considered as robust models since they describe not only the interface elastic behaviour but also irreversible phenomena such as damage and/or plasticity. They enable a refined evaluation of the cohesive stresses distribution along the interface during monotonous loading of the joint. These models are defined by the use of a traction separation (TS) laws. Their shapes and corresponding parameters are usually empirically chosen according to the expected global behavior of the material (i.e. brittle, ductile) and then adjusted to the experimental measurements until a good agreement is found with an analytical or numerical model [2]. In the literature, the most frequently used TS law shapes are the bilinear one for brittle adhesive and trilinear one for ductile adhesive.

However, the prediction of both crack initiation and propagation regimes may still suffer from a lack of precision mainly because the TS law shape is chosen empirically rather than measured. It was indeed showed that the TS law shapes and its chosen parameters have an impact on the predicted mechanical response of the specimen, especially for ductile adhesives [3]. This is why an extensive work has been ongoing for the development of specialized experimental techniques for measuring accurately the interface separation law. These new characterization protocols lead to the use of new specimens and loading systems such as the DCB fixture developed by Sorensen et al. [4] where the specimen is loaded with opposite bending moments and which enable the direct determination of the TS through the differentiation of the J integral. Adherends' deformation can also be measured using optical [5] or resistive strain gauges [6]. As it enable a precise location of the crack tip but can also be used for the direct identification of the CZM through the differentiation of the backface strain signal evolution. Contrary to other methods with the backface strain monitoring (BFS) technique the interface behaviour is revealed during the crack propagation regime rather than during the initiation regime. Thus, direct inversion techniques have being proposed for the CZM reconstruction from the experimental data obtain with BSM and J(θ,Δ) techniques but they necessitate the use of heavy data reduction scheme. On the contrary, inverse methods are being used to analyse P(Δ) measurements. In these cases, some assumptions are made on the TS shape which must be set arbitrary and which can lead to errors on latter predictions.

Therefore, this contribution aims at proposing a systematic procedure to evaluate the sensibility of the three mechanical fields (P(Δ),J(θ,Δ), BSM) used in the inverse evaluation of the TS law parameters such as interface stiffness, strength and fracture energy. A simple semi-analytical model of a DCB experiment considering non-linear interface behaviour is implemented to generate synthetic experimental data with known interface behaviour. Some Gaussian noise is added to the data then a Levenberg-Marquart minimization algorithm is used to minimize an error function and identify the TS law parameters. The confidence domains for the group of fitted parameters are obtained at the end of the minimization procedure for all three measurement-techniques. It can be used for the evaluation of the identification quality and techniques' comparison.

## 2 DCB MECHANICAL RESPONSE: ANALYTICAL MODEL

### 2.1 Nonlinear interface behavior

The DCB specimen, illustrated in Figure 1, is modelled as two Timoshenko beams having rectangular cross section (width: *w*, thickness: *t*). The length of the bonded part is *L*. On the right end of the specimen the two slabs are left unbonded over a distance equal to *a* and considered as the initial crack length. The adhesive layer is represented by bilinear TS law whose stress versus displacement jump, v, are given by equation 1 to 3:

$$\sigma = \frac{2E_a^*}{t_a} v(x) \qquad v < t_a \frac{\varepsilon_e}{2} \tag{1}$$

$$\sigma = \frac{\sigma_{max}}{v_e - v_p} (v_p - v(x)) \qquad t_a \frac{\varepsilon_e}{2} < v < t_a \frac{\varepsilon_p}{2} \tag{2}$$

$$\sigma = 0 \qquad v > t_a \frac{\varepsilon_p}{2} \tag{3}$$

The equation 1 corresponds to the elastic regime with $E_a{}^*$ being the adhesive apparent Young's Modulus and $t_a$ being the bondline thickness. In the present article, only softening behaviour is considered using the classical TS law. The interface starts damaging when the peel stress reaches $\sigma_{max}$ value or equivalently when the relative displacement between adherends reaches the value $v_e = \frac{t_a}{2}\varepsilon_e$ . Full damage and decohesion of the interface is reached when the adhesive deformation is equal to $\varepsilon_p$ so that relative displacement of both adherent is equal to $v_p = \frac{t_a}{2}\varepsilon_p$.

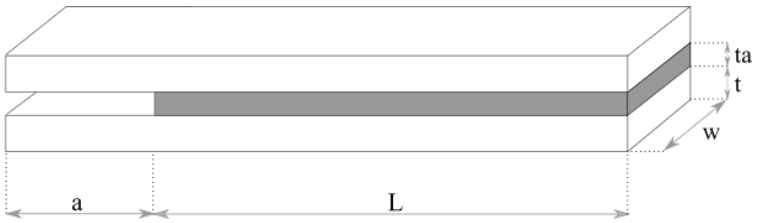


Figure 1: DCB specimen geometric data considered in the analytical model

Due to the specimen and loading conditions symmetry, the overall specimen behaviour is determined only from the one of the upper adherend. First, the local beam equilibrium should be considered:

$$\frac{dM(x)}{dx} + T(x) = 0 \tag{4}$$

$$\frac{dT(x)}{dx} - w\sigma(x) = 0 \tag{5}$$

Then, the Timoshenko beams constitutive equations should be taken into account:

$$M(x) = EI\frac{d\varphi(x)}{dx} \tag{6}$$

$$T(x) = \kappa GS\left(\frac{dv(x)}{dx} - \varphi(x)\right) \tag{7}$$

*M* and *T* are the beam local bending moment and shear force and $\sigma(x)$ is the local peel stress. $v(x)$ are $\varphi(x)$ respectively the beam deflection and cross section rotation. The adherend's material parameters *E* and *G* are respectively the Young's modulus and the shear modulus. $S = wt$ corresponds to the beam cross section area. In case of a rectangular cross section the quadratic moment is computed as $I = \frac{wt^3}{12}$ and the shear correction coefficient is approximately $\kappa = \frac{5}{6}$. The combination of equation 1 to 7 gives two ordinary differential equations. The first one is for the elastic part (eq. 8) and second one for the softening part (eq. 9):

$$\frac{d^4\sigma(x)}{dx^4} - \frac{k_I}{\kappa GS}\frac{d^2\sigma(x)}{dx^2} + \frac{k_I}{EI}\sigma(x) = 0 \qquad \text{with } k_I = w\frac{2E_a^*}{t_a} \tag{8}$$

$$\frac{d^4\sigma(x)}{dx^4} + \frac{k_{II}}{\kappa GS}\frac{d^2\sigma(x)}{dx^2} + \frac{k_{II}}{EI}\sigma(x) = 0 \qquad \text{with } k_{II} = \frac{w\sigma_{max}}{(v_p - v_e)} \tag{9}$$

Where $k_I$ and $k_{II}$ are respectively the interface tangent stiffness in the elastic and softening bondline regions. Then, the general expression of the adherend deflection evolution along the bondline is given by:

$$\sigma(x) = \sum_{i=1}^{2} A_i e^{\lambda^* i x} + B_i e^{-\lambda^* i(L-x)} + Cst \tag{10}$$

$$\lambda_j = \left(\frac{k_j}{EI}\right)^{1/4} \qquad j \in [I, II] \tag{11}$$

$$\varepsilon = \frac{\sqrt{kEI}}{2\kappa GS} \tag{12}$$

$$\lambda^*{}_i = \lambda_j \sqrt{\varepsilon \pm \sqrt{\varepsilon^2 - 1}} = \lambda \alpha_i \qquad i \in [1,2] \text{ and } j \in [I, II] \tag{13}$$

With Cst and λ respectively equal to zero and $\lambda_I$ in the elastic region and equal to $\sigma_0$ and $\lambda_{II}$ in the softening region. All other cohesive forces and displacement evolutions are obtained by integrating equations 4 to 7, considering continuity in between the elastic and softening region and the following boundary conditions:

$$M(x = 0) = aP \tag{14}$$

$$T(x = 0) = P \tag{15}$$

The simulation of crack initiation and propagation is a three-step process. First elastic calculations are effected considering only elastic region along the adhesive. The end of elastic loading regime is reached when $v(x = 0) = v_e$. Then, the crack initiation is simulated by considering fixed position of the crack tip but increasing the size of the softening region until $v(x = 0) = v_p$. Finally, the crack propagation period is simulated by considering increasing value of $a$ and by updating at each crack position the softening region length with an iterative process. The results of such calculation give access to the load versus displacement and J(θ,δ) evolutions during the whole test Then, for a given opening displacement the shear forces, bending moment, adherends deflection and rotation is obtained along the overlap.

### 2.2 Traction-separation law measurement techniques

To illustrate the need for TS law identification techniques, some DCB test simulations are carried out for three bilinear TS laws. The DCB test specimen characteristics are presented below considering triangular TS law which are defined by the adhesive effective modulus $E_a^*$, the maximum stress $\sigma_{max}$, and the critical energy release rate $G_c$. The TS parameters values are indicated in **Erreur ! Source du renvoi introuvable.**. The first triplet will later be used as nominal values.

| Reference | $E_a^*$ (MPa) | $\sigma_{max}$ (MPa) | $G_c$ $(N/mm)$ |
|---|---|---|---|
| TS1 | 146 | 14 | 1.4178 |
| TS2 | 20 | 11 | 2 |
| TS3 | 300 | 20 | 1 |

Table 1: Traction separation laws parameters

These TS laws can be displayed as stress function of displacement jump at crack tip. In order to emphasize the importance of the TS law on the bonded specimen mechanical response, these three laws will be used to compare the response of the DCB test obtained from commonly used measurements method.

#### 2.2.1 From load versus displacement measurement

The first method proposed to evaluate TS law from DCB experiment is based on the analysis of the force, P, versus opening displacement evolution, Δ. Since the original analysis of DCB test, these data are systematically measured as it enables the evaluation of the interface critical SERR which is based on compliance measurement evolution. As it can be seen on Figure 2(a), P(Δ) curve is typically split into three parts corresponding to the three distinct regime of the CZM. The first one is linear. Then once the adhesive begins to soften, the force keeps increasing but nonlinearly and finally, when the

critical energy release rate is reached crack propagation begins. This part can also be predicted using the SBT method presented in equation 16.

$$P = \left(\frac{4E_s I_n}{9}\right)^{\frac{1}{4}} (wG_c)^{\frac{3}{4}} (\Delta)^{-\frac{1}{2}} \tag{16}$$

The P(Δ) evolutions obtained with the three TS laws are presented in Figure 2(b) showing how the TS shape may affect the overall response of the specimen during testing. It appears that it is the critical energy release rate that has the most impact on the curve.

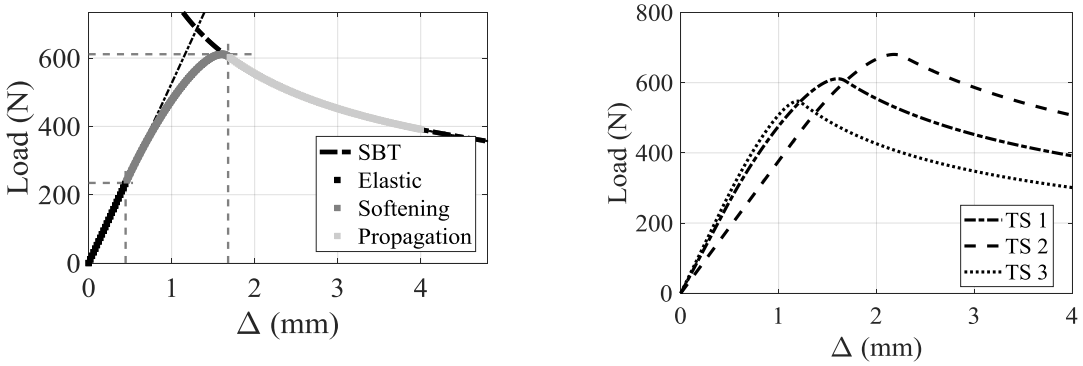


(a) (b)

Figure 2: Load-displacement curves: (a) Division of the P(Δ) curve according to the TS law phase; (b) Impact of the TS law on the P(Δ) response.

### 2.2.2 From J(θ,Δ) measurement

Gunderson and al. [8] proposed to evaluate the J integral evolution during the DCB test directly by measuring the specimen end rotation together with the applied load. In addition, Anderson et al proposed a solution for adherends having an Euler-Bernoulli behaviour [9]. But it can be extended to adherends behaving as Timoshenko beams as well. If the integral J evaluation is made by using the full specimen boundary as the contour, it can be expressed as:

$$J = \frac{2}{w}\left[P\theta + \frac{P^2}{2\kappa GS}\right] \tag{17}$$

Where P and $\theta$ are respectively the load and the rotation at loading point. The geometric parameters $w$, $S$ and $\kappa = \frac{5}{6}$ corresponds to the adherends width, the adherends' cross section area and shear correction coefficient. Lastly, $G$ represents the shear modulus. The integral J can then be plotted as a function of the opening displacement at loading point. The J(θ,Δ) evolution reduces to three different regions, the elastic ad softening ones showing parabolic evolutions but with opposite curvature and the third one being constant when J remains stationary (Figure 3(a)). From Figure 3(b), it appears once again that it is the critical energy release rate that has the most impact on the curve.

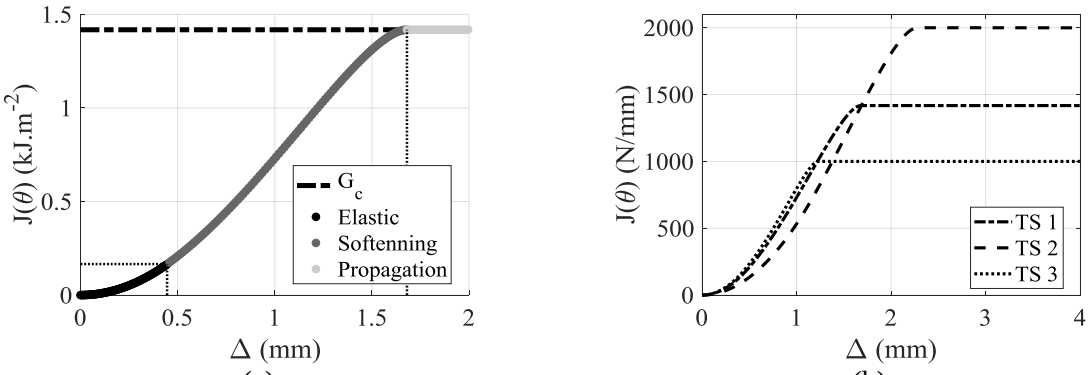


(a) (b)

Figure 3: Integral J function of the opening at loading point: (a) Division of the J(θ,Δ) curve according to the TS law phase; (b) Impact of the TS law on the J(θ,Δ) response.

### 2.2.3 From gauges measurement

Resistive gauges can be placed on the adherend's upper side. The measurement of the slabs deformation gives insight on the stress state of the adhesive bond directly underneath the gauges. They measure the local longitudinal strain which is proportional to the local bending moment M:

$$\varepsilon_s = \frac{M}{E_s I_n}\frac{t}{2} \tag{18}$$

It also depends on the adherends' Young modulus $E_s$, their quadratic moment $I_n$ and their thickness t. The gauge evolution can also be used for a direct evaluation of cohesive stresses evolution along the bondline by using the relation:

$$\sigma = -2\frac{EI}{wt}\frac{d^2\varepsilon}{dx^2} \tag{19}$$

The gauges response is an indicator of the stress state of the adhesive below which phases are given by Figure 4(a). It is worth noticing that the adherend deformation is maximal when the crack tip is close to the gauge. Figure 4(b) illustrates the influence of the TS law on the gauge mechanical response.

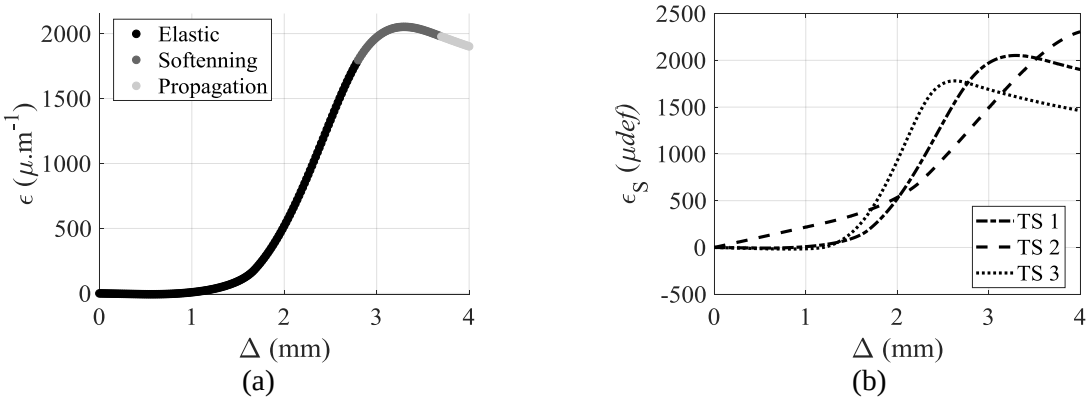


Figure 4: Gauges deformation function of the opening at loading point: (a) Division of the Gauge curve according to the TS law phase; (b) Impact of the TS law on the Gauge response.

## 3 CONFIDENCE INTERVALS METHODOLOGY

### 3.1 $\chi^2$ minimization and confidence intervals

Obtaining model parameters from a set of experimental data can be achieved with different techniques. The most common one consists in minimizing an error function which may exhibit significantly non-linear behaviour. In the following, least square minimization is performed considering the Chi square, $\chi^2$, function defined with relation :

$$\chi^2(a) = \sum_{i=1}^{n_d}\left[\frac{Y(t_i) - \hat{Y}(a,t_i)}{\sigma_Y(t_i)}\right]^2 \tag{20}$$

In equation 20, $Y(t_i),\ i=\{1,\ldots,n_d\}$ represent the $n_d$ measured data used to identify the $a_k$, with $k=\{1,\ldots,p\}$ the different parameters. $\hat{Y}$ are the corresponding theoretical data obtained with the model. The term in the sum are weighted by the measurement error on the experimental data. This function is minimized using steepest gradient technique such as Levenberg-Marquart algorithm until the minimum $\chi^2$value is found and the corresponding optimum set of parameters is determined.

Once $a$, the optimal parameters' vector is found, parameters confidence intervals can be evaluated by analysing the $\chi^2$ function evolution near the minima. Indeed, the small variation of one or several

parameters will lead to an increase of the $\chi^2$ value, a steep increase meaning a high sensibility to any parameter fluctuation and then high reliability of the identification process. First evaluation of the confidence interval is obtained by performing second order Taylor expansion of the $\chi^2$ function near the minima. It results in a simple quadratic approximation of the error function close to the optimised parameters, $a^{opt}$, as follow:

$$\chi^2(a - a^{opt}) = \chi^2(x) - d.\,\delta a + \delta a.\,C^{-1}.\,\delta a \tag{21}$$

with

$$\delta a_k = a_k - a_k{}^{opt} \tag{22}$$

$$d_k = \frac{\partial \chi^2}{\partial a_k} = -2 \sum_{i=1}^{n_d} \left[ \frac{Y(t_i) - \hat{Y}(a, t_i)}{\sigma_Y^2(t_i)} \right] \frac{\partial \hat{Y}(a, t_i)}{\partial a_k} \tag{23}$$

and

$$C_{kl}{}^{-1} = \frac{\partial^2 \chi^2}{\partial a_k \partial a_l} = \sum_{i=1}^{n_d} \frac{1}{\sigma_Y^2(t_i)} \left[ \frac{\partial \hat{Y}(a, t_i)}{\partial a_k} \frac{\partial \hat{Y}(a, t_i)}{\partial a_l} \right] \tag{24}$$

In Eq. 21, the vector d is equal to zero, since for the optimum sets of parameter the Chi-square function is minimum and the gradients are equal to zero. The complete expression of the second order term coefficient is given by relation:

$$\frac{\partial^2 \chi^2}{\partial a_k \partial a_l} = 2 \sum_{i=1}^{n_d} \frac{1}{\sigma_{Y(t_i)}^2} \left[ \frac{\partial \hat{Y}(a, t_i)}{\partial a_k} \frac{\partial \hat{Y}(a, t_i)}{\partial a_l} - \left( Y(t_i) - \hat{Y}(a, t_i) \right) \frac{\partial^2 \hat{Y}(a, t_i)}{\partial a_k \partial a_l} \right] \tag{25}$$

However, the term $\sum_{i=1}^{n_d} Y(t\_i) - \hat{Y}(a, t\_i)$ tends to zero for large $n_d$ value since it represents the average noise value when the model is exact [10]. Then, the second order term reduces to the sole covariance matrix:

$$C = \sigma^2 (JJ^T)^{-1} \tag{26}$$

with J corresponding to the sensitivity function:

$$J = [J_k(t_i)] = \frac{\partial \hat{Y}(a, t_i)}{\partial a_k} \tag{27}$$

Assuming the variance, $\sigma^2$, is constant for all data points , it can be estimated with the relation 28 [11]:

$$\sigma^2 = \frac{\sum_{i=1}^{n_d} \left( Y(t_i) - \hat{Y}(p, t_i) \right)^2}{n_d - n_p} \qquad i \in [1{:}\, n_d] \tag{28}$$

The confidence intervals on the identified parameters can be obtained from the analysis of the $\chi^2$ function evolution near the minimum. Indeed, for a given reliability and number of degree of freedom ($n_d$ minus identified parameters, $n_p$) the variation $\Delta\chi^2$ of the error function due to parameters variation $\delta a$ should be less than the value defined by $\chi^2$ function values table. From the asymptotic analysis and expression, these confidence intervals can be estimated once the covariance matrix has been determined:

$$\Delta\chi^2 = \delta a\, C^{-1} \delta a \tag{29}$$

The envelope of the confidence domain is then represented by an ellipse, when two parameters are identified. Likewise for three parameters it is represented as an ellipsoid. However, the real shape of the confidence region might be different if the minimization problem is highly nonlinear and determined with the condition:

$$\Delta\chi^2(\delta a\ ) = C^{st} \tag{30}$$

For visualisation and analysis purposes, it might be needed to reduce the number of parameters used. As joint confidence regions are larger than individual intervals for the same confidence. Moreover, some parameters might be irrelevant for the analysis as they are not affected and do not infer with the other desired parameters. It is then possible to project the covariance matrix on a lesser dimension. Equation **Erreur ! Source du renvoi introuvable.**29 can then be expressed as

$$\Delta\chi^2(IC\%, \nu\ ) = \delta a\ {C_{proj}}^{-1}\delta a' \tag{31}$$

The Chi-square distribution value is tabulated for $n_p$ degrees of freedom, $\delta a'$corresponds to the vector of interest parameters whose length is $\nu < n_p$. $C_{proj}$ is the projected covariance matrix where rows and columns not corresponding to the parameters of interest are removed. This can be extended to the calculation of confidence intervals for each parameter individually which is given by:

$$\delta a_i = \pm\sqrt{\Delta\chi^2(IC\%, 1)}\sqrt{C_{ii}} \tag{32}$$

The confidence region analysis can also give information on the correlation of the parameters. It can be determined using two different methods. First, a correlation matrix can be determined using the covariance matrix [12]. It will give access to a normalized estimation of the linear correlation between each pair of parameters, diagonal parameters being equal to one.

$$corr(i.j) = \frac{C(i,j)}{\sqrt{C(i,i)}\sqrt{C(j,j)}} \qquad (i,j) \in [1{:}n_p] \tag{33}$$

From a technical standpoint, the curve fitting is performed using the lsqnonlin function implemented in Matlab using the Levenberg-Marquardt algorithm. In order to obtain a more accurate optimization, the gradients were estimated with central finite differences.

### 3.2 Model definition

The analytic model, presented in section 1.1, is used to simulate a DCB specimen. Its geometric and material characteristics are summarized in Table 2. The adhesive is chosen as 247µm-thick and is implemented using a bilinear cohesive zone model. Its parameters of interest are arbitrarily chosen as: the initial modulus the maximum stress and the displacement jump at propagation: $a = [E_a, \sigma_{max}, v_p]$. **Erreur ! Source du renvoi introuvable.**Table 2 includes the chosen nominal parameters and the associated critical energy release rate in mode I as well as the surface area under the linear part, respectively termed $G_c$ and $Y_0$.

| **Adherends** | | **Adhesive TS law** | |
|---|---|---|---|
| Total length (mm) | 180 | $E_a$ (MPa) | 146 |
| Overlap length (mm) | 130 | $\sigma_{max}$ (MPa) | 14 |
| Initial crack length (mm) | 50 | $v_p$ (µm) | 101.27 |
| Thickness (mm) | 10 | $Y_0$ (N/mm) | 0.67 |
| Width (mm) | 15 | $G_c$ (N/mm) | 1.42 |
| Young modulus (GPa) | 70 | Thickness (µm) | 247 |
| Poisson ratio ( - ) | 0.3 | | |

Table 2: DCB specimen geometric, materials characteristics and CZM properties

The minimization and interval region procedure were carried out for each mechanical response that can be obtained on a DCB test (i.e. P(Δ), J(θ,δ), Gauges). However, for clarity purpose, the process will only be detailed for the force-displacement curve. The experimental data are then generated from the known nominal response on which a normal noise has been introduced. Each experimental curve contains 201 points taken for the same opening displacement value. This numerical noise represents the experimental data variations caused by errors in the measurement chain (i.e. load captors, gauges...)

[12] and is tailored for each mechanical response. It is generated as a normal distribution whose mean is equal to zero and whose standard deviation is approximately 1% of the maximal mechanical response. The noise distribution is chosen equal to 10 N for P(Δ), 10 kJ/m² for J(θ,Δ) and 20 µdef for the gauge.

The Chi-square minimization is performed on synthetic experimental data in order to determine the parameters triplet. The optimization is effected 12 times for each mechanical response with a new random noise to validate the process**.** To identify the confidence regions, sensitivity functions are determined analytically using equation 27. Mechanical responses are computed for a ±5% variation of each parameter.

### 3.3 Application to the force versus displacement measurement

The P(Δ) synthetic experimental data and its optimization results are displayed in Figure 5(a). Load-displacement sensitivity function for the force-displacement curve are illustrated in Figure 5(b), the normalized force gradient is displayed as a function of the opening at loading point Δ. The graph is separated in 3 zones that represent the evolution of the cohesive zone model. The first area going from $\Delta = 0\ mm$ to $\Delta = 0.5\ mm$ corresponds to the adhesive elastic behaviour. The second part from $\Delta = 0.5\ mm$ to $\Delta = 1.5\ mm$ represents its softening behaviour and the last part the crack propagation. It appears that the modulus has its biggest influence during the elastic part and then decreases until it reaches zero when the propagation start. That is to say that the adhesive modulus has no effect on the propagation phase of the DCB test whereas this propagation phase provides the largest number of experimental points. On the other hand, the maximal stress and displacement jump have no impact in the elastic phase, little impact during the 2nd part but are really significant during the propagation phase. Moreover, as they appear and behave similarly they will be difficult to distinguish from each other. Meaning that they will be strongly correlated.

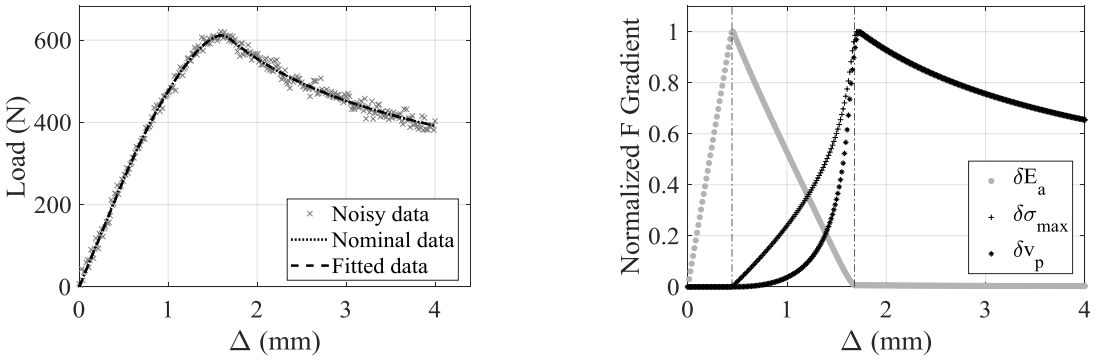


Figure 5: (a) Synthetic measurements data with its optimisation result; (b) Normalized sensitivity functions for the load displacement mechanical response

Once the sensitivity functions and the standard deviation between the optimized model data and the experimental data are computed, the covariance matrix can be determined. It is possible to draw the confidence region in three-dimension and projected on 2-parameters plane. The confidence regions at 95% of the force-displacement curves are illustrated in Figure 6. The ellipsoid and ellipses are centred on the nominal value. As expected, the individual confidence intervals are smaller than the joint regions in two dimensions. It appears that the 95% confidence intervals (i.e. individual) for the modulus is comprised between 127.3MPa and 164.7 MPa, for the maximal stress between [13.7, 14.5] MPa and for the displacement jump between [98.2, 104.4] µm. Moreover, in order to assess the quality of the minimization and confidence regions, the Chi-square optimization has been carried out 12 times for experimental data on which was applied a new random noise. The results of these minimizations are illustrated in Figure 6 as grey diamonds. It can be noticed that they are all included in the confidence regions and intervals which is a quality assurance of the minimization procedure and shows that the results are reproducible.

The figure also highlights the coupling between the parameters through the ellipses angle of inclination. Such coupling between the parameters is computed with the correlation matrix (eq. 33), in the force-displacement case it gives:

$$corr = \begin{bmatrix} 1 & -0.51 & 0.50 \\ -0.51 & 1 & -0.99 \\ 0.5 & -0.99 & 1 \end{bmatrix} \tag{34}$$

The correlation matrix indicates that the variation of the maximal stress and displacement jump at propagation are so highly correlated that the variation of one can be quasi entirely compensated by the other one, making the identification less reliable. To reduce this constraint, other set of parameters triplet could be used such as critical energy release rate instead of $v_p$.

Moreover, the confidence regions and intervals should be carefully analysed since the method uses quadratic approximation when it is not necessarily true. Thus, the real confidence regions might not be regular ellipses and confidence intervals in one dimension might not be symmetric. However, this method enables the easy comparison of different mechanical responses that can be used to determine the adhesive traction separation law parameters.

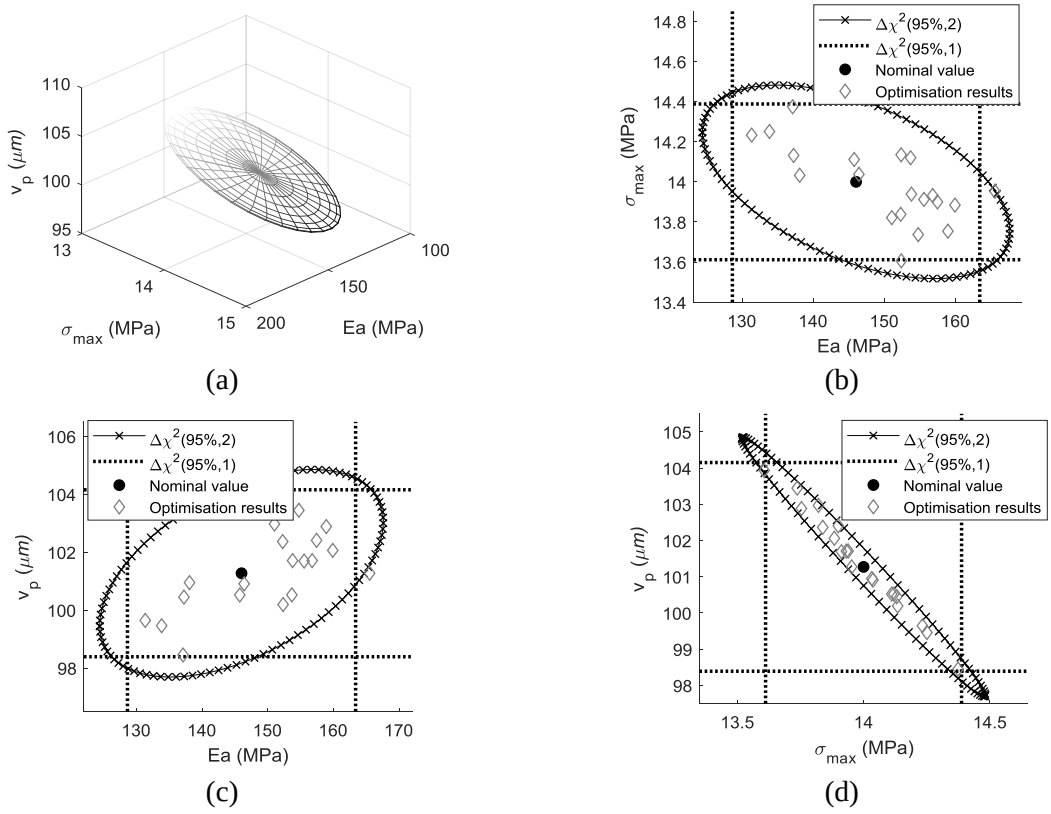


Figure 6: Confidence regions at 95% for the Force-displacement response: (a) 95% confidence ellipsoid; (b) 95% confidence ellipse for $E_a$ and $\sigma_{max}$; (c) 95% confidence ellipse for $E_a$ and $v_p$; (b) 95% confidence ellipse for $\sigma_{max}$ and $v_p$

## 4 METHODS COMPARISON

The most straightforward results to analyse are the confidence intervals for each parameter individually. They are symmetric and centred around the nominal value. Therefore, the comparison between the methods will only be made with the interval radius. The results for every method and every parameter for a 95% confidence interval are summarized in Table 3. It appears that the gauge is the method that has the smallest confidence interval for the modulus. However, the J(θ,Δ) method gives the best results for $\sigma_{max}$ and $v_p$.

| Method | $E_a$ (MPa) | $\sigma_{max}$ (MPa) | $v_p$ (µm) |
|---|---|---|---|
| P(Δ) | 18.70 | 0.42 | 3.10 |
| J(θ,δ) | 13.22 | 0.17 | 1.21 |
| Gauge | 10.78 | 0.55 | 4.03 |

Table 3: 95% confidence intervals comparison

Another insight on the differences between the methods is given by the correlation matrix (Table 4). Indeed, for each method parameters coupling appears to be different but follows the same trends. The couple $\sigma_{max}/\delta_p$ appears to be strongly correlated for every method. It implies that during the minimisation their correct value might not have been found accurately as a small variation of one compensates the deviation of the other. The two other couples are moderately correlated. The smallest coupling is found for the P(Δ) method.

| Method | $E_a/\sigma_{max}$ | $E_a/\delta_p$ | $\sigma_{max}/\delta_p$ |
|---|---|---|---|
| P(Δ) | -0.510 | 0.500 | -0.990 |
| J(θ,δ) | -0.639 | 0.635 | -0.996 |
| Gauge | -0.751 | -0.747 | -0.998 |

Table 4: Correlation between the parameters couple

The visual analysis of the confidence ellipses given by the projection of the ellipsoid on two dimensions planes gives complementary information (Figure 7). The correlation between the parameters is represented by the ellipses inclination. The smallest interval regions are obtained for the J(θ,Δ) method.

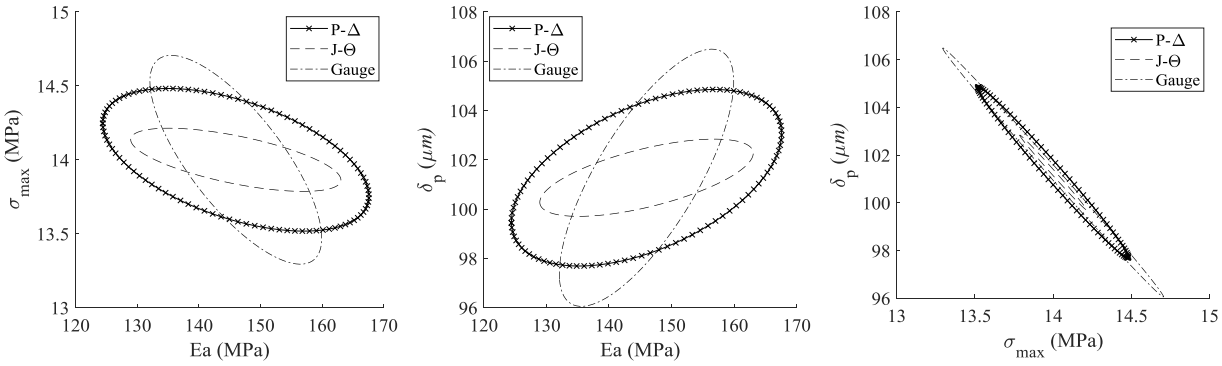


(a) (b) (c)

Figure 7: Comparison of two-dimensions 95% interval regions comparison: (a) Modulus and maximal stress plane; (b) Modulus and displacement jump at propagation plane; (c) Maximal stress Modulus and displacement jump at propagation plane.

Moreover, as the DCB test was designed to determine the critical energy release rate $G_c$, another verification can be done using its evaluation for the 95% confidence ellipsoid surface. All methods except the gauges give a prediction with less than 0.05% variation from the nominal value, which is equal to 1.41780 N/mm and the closest result is obtained for the J(θ,δ) method with 1.41766 N/mm.

## 5 CONCLUSION

The Chi-square analysis of measurements method used on DCB test enabled the implementation of a comparison technique through the development of a numerical Chi-square analysis. It showed that in order to determine the parameters of an arbitrarily chosen TS law shape with an inverse method, the smallest confidence regions are given by the J(θ,Δ) method. This method is then very convenient for

both the simplicity of experimental implementation, and its straightforward experimental data reduction method. However, it should be noticed that the use of the J integral needs to comply with a constrained theoretical framework such as not time dependent behaviour. Therefore, using other techniques might be of use so as to validate the consistency of the identification results with supplementary set of experimental data. Also, this analysis was restricted to the triangular TS shape. Other CZM shall be considered next, first to generalize the present results but also to check that the data reduction technique are able to discriminate different TS shape.

## ACKNOWLEDGEMENTS

As part of the collaborative project S3PAC (FUI 21), this work was co-funded by BPI France, the Occitanie region and the Nouvelle Aquitaine region.

## REFERENCES

[1] N. Chandra, H. Li, C. Shet et H. Ghonem, «Some issues in the application of cohesive zone models for metal--ceramic interfaces,» *International Journal of Solids and Structures,* vol. 39, pp. 2827-2855, 2002.

[2] C. D. M. Liljedahl, A. D. Crocombe, M. A. Wahab et I. A. Ashcroft, «Modelling the environmental degradation of adhesively bonded aluminium and composite joints using a CZM approach,» *International Journal of Adhesion and Adhesives,* vol. 27, pp. 505-518, 2007.

[3] M. Alfano, F. Furgiuele, A. Leonardi, C. Maletta et G. H. Paulino, «Mode I fracture of adhesive joints using tailored cohesive zone models,» *International journal of fracture,* vol. 157, pp. 193-204, 2009.

[4] B. F. Sørensen, A. Horsewell, O. Jørgensen, A. N. Kumar et P. Engbæk, «Fracture resistance measurement method for in situ observation of crack mechanisms,» *Journal of the American Ceramic Society,* vol. 81, pp. 661-669, 1998.

[5] D. Sans, J. Renart, J. Costa, N. Gascons et J. A. Mayugo, «Assessment of the influence of the crack monitoring method in interlaminar fatigue tests using fiber Bragg grating sensors,» *Composites Science and Technology,* vol. 84, pp. 44-50, 2013.

[6] J. Jumel, N. B. Salem, M. K. Budzik et M. E. R. Shanahan, «Measurement of interface cohesive stresses and strains evolutions with combined mixed mode crack propagation test and Backface Strain Monitoring measurements,» *International Journal of Solids and Structures,* vol. 52, pp. 33-44, 2015.

[7] H. Haddadi et S. Belhabib, «Use of rigid-body motion for the investigation and estimation of the measurement errors related to digital image correlation technique,» *Optics and Lasers in Engineering,* vol. 46, pp. 185-196, 2008.

[8] J. D. Gunderson, J. F. Brueck et A. J. Paris, «Alternative test method for interlaminar fracture toughness of composites,» *International Journal of Fracture,* vol. 143, pp. 273-276, 2007.

[9] T. Andersson et A. Biel, «On the effective constitutive properties of a thin adhesive layer loaded in peel,» *International Journal of Fracture,* vol. 141, pp. 227-246, 2006.

[10] W. H. Press, S. A. Teukolsky, W. T. Vetterling et B. P. Flannery, Numerical recipes in C, vol. 2, Cambridge university press Cambridge, 1982.

[11] S. Marsili-Libelli, S. Guerrizio et N. Checchi, «Confidence regions of estimated parameters for ecological systems,» *Ecological Modelling,* vol. 165, pp. 127-146, 2003.

[12] S. Hartmann et R. R. Gilbert, «Identifiability of material parameters in solid mechanics,» *Archive of Applied Mechanics,* vol. 88, pp. 3-26, 2018.